arXiv:astro-ph/0410617v2 21 Jan 2005

Diffractive Interaction and Scaling Violation in $pp \to \pi^0$ Interaction and GeV Excess in Galactic Diffuse Gamma-Ray Spectrum of EGRET

Tuneyoshi Kamae[1], Toshinori Abe and Tatsumi Koi

Stanford Linear Accelerator Center, Menlo Park, CA 94025

kamae@slac.stanford.edu

ABSTRACT

We present here a new calculation of the gamma-ray spectrum from $pp \to \pi^0$ in the Galactic ridge environment. The calculation includes the diffractive p-p interaction and incorporates the Feynman scaling violation for the first time. Galactic diffuse gamma-rays come, predominantly, from $\pi^0 \to \gamma\gamma$ in the sub-GeV to multi-GeV range. Hunter et al. found, however, an excess in the GeV range ("GeV Excess") in the EGRET Galactic diffuse spectrum above the prediction based on experimental $pp \to \pi^0$ cross-sections and the Feynman scaling hypothesis. We show, in this work, that the diffractive process makes the gamma-ray spectrum harder than the incident proton spectrum by ~ 0.05 in power-law index, and, that the scaling violation produces $30-80\%$ more π^0 than the scaling model for incident proton energies above 100 GeV. Combination of the two can explain about a half of the "GeV Excess" with the local cosmic proton (power-law index ~ 2.7). The excess can be fully explained if the proton spectral index in the Galactic ridge is a little harder (~ 0.2 in power-law index) than the local spectrum. Given also in the paper is that the diffractive process enhances e^+ over e^- and the scaling violation gives $50-100\%$ higher $\bar{p}$ yield than without the violation, both in the multi-GeV range.

Subject headings: gamma-rays: observation — gamma-rays: theory — diffuse radiation — cosmic rays — ISM: general

---

[1]Also with Kavli Institute for Particle Astrophysics and Cosmology, Stanford University, Menlo Park, CA 94025

1. Introduction

Gamma-rays from neutral pions produced by cosmic-ray proton interactions with ISM have been predicted to dominate the diffuse Galactic emission in the sub-GeV to GeV band since 1960's. Early pioneers including Ginzburg (1967) and Hayakawa (1969) have estimated the gamma-ray flux from π^0 together with other important mechanisms around that time.

First quantitative observation-based studies of the diffuse gamma-ray spectrum covering the sub-GeV and GeV band were made, eg. by Strong et al. (1978), Stephens & Badhwar (1981), Dermer (1986), and Stecker (1989). They compared the data from COS-B (Bignami et al. 1975) with their models based on experimental $pp \rightarrow \pi^0$ data from accelerators, their extension to higher energies on the Feynman scaling hypothesis (Feynman 1969), estimations on cosmic ray proton and electron fluxes, and the ISM distribution obtained by radio surveys. Within the uncertainties in the data and modeling, the studies cited above concluded that gamma-rays from π^0 are a dominant component in the Galactic ridge spectrum above 100 MeV. The bremsstrahlung emission by e^+/e^- off ISM atoms and the inverse-Compton scattering of infra-red and optical photons by e^+/e^- are also expected to contribute significantly in the sub-GeV to GeV energy range (Hayakawa 1969; Murthy & Wolfendale 1993; Schoenfelder 2001)

The limited statistics and energy coverage of the COS-B gamma-ray data permitted only a crude consistency check of the $pp \rightarrow \pi^0 \rightarrow \gamma$ hypothesis within a factor ~ 2 and left large ambiguity on the mix of emission mechanisms (Stephens & Badhwar 1981). The spatial distribution of the energy-integrated gamma-ray intensity, on the other hand, gave a higher statistical accuracy on which Mayer-Hasselwander et al. (1982), Strong et al. (1982), Bloemen et al. (1984), Bloemen et al. (1985), and others set the path to the Galactic gamma-ray astronomy. We refer to Murthy & Wolfendale (1993), Schoenfelder (2001), and Schlickeiser (2002) for general references on the topics of this work.

When the much improved data obtained with EGRET (Thompson et al. 1993) were studied by Bertsch et al. (1993) and Hunter et al. (1997), an excess of about $\times(1.5 - 2)$ became apparent in the data in the GeV band relative to the Galactic gamma-ray emission models cited above. This excess is visible along the entire Galactic plane ($-10 < b < 10$ deg. and $-90 < \ell < +90$ deg.) but most pronounced in the central region of the plane ($-40 < \ell < +40$ deg.). Here b and ℓ are the Galactic latitude and longitude, respectively. In literature, the excess is referred to as the "GeV Excess".

Mori (1997) studied the diffuse gamma-ray emission by using Monte Carlo p-p interaction simulators devloped for accelerator experiments and confirmed that the EGRET spectrum can not be reproduced with the conventional cosmic proton spectrum.

Strong and Moskalenko developed a computer program, GALPROP, where the cosmic ray propagation and interaction are numerically calculated in a model Galaxy to obtain the spatial distribution and spectrum of secondary particles including gamma-rays and radio isotopes (Strong & Moskalenko 1997, 2001). The diffuse Galactic gamma-ray spectra have been calculated separately for the π^0 decay, bremsstrahlung, and inverse-Compton with various parameter settings of GALPROP by Strong et al. (2000). They noted that: a) the local interstellar spectra of electrons and protons (power-law index ≥ 2.5 above $10-20$ GeV) do not reproduce the gamma-ray spectrum along the Galactic plane observed by EGRET; b) a very hard electron spectrum (power-law index ~ 1.8) and a modified nucleon spectrum will be needed to minimize the difference between the prediction and the data in the GeV band; and c) the GeV excess in the central Galactic ridge can not be reproduced within the constraint on the proton spectral index imposed by recent cosmic proton measurements and the limit on the electron spectral index (~ 1.9) from radio and local cosmic ray observations. They noted that the excess persists at higher Galactic latitude ($|\ell| > 5$ deg).

Buesching et al. (2001) have also noted that the EGRET spectrum is incompatible with the locally measured cosmic proton spectrum.

The GeV Excess has led to new optimizations of the Galactic gamma-ray emission models and speculations on possible new gamma-ray sources in the Galaxy. One choice is to assume a harder proton spectrum in the Galactic ridge region as has been noted by Mori (1997). Another choice is to assume a much higher electron flux with a broken power-law spectrum in the Galactic ridge (Strong et al. 2004). Buesching et al. (2001) has proposed to introduce a mix of spectral indices for protons which leads to a convex gamma-ray spectrum similar to that observed by EGRET. Possible contributions of unidentified pulsars (Pohl et al. 1997) and dark-matter particle annihilation (de Boer et al. 2003; Cerarini et al. 2004) have also been studied.

We came to note that all calculations of the Galactic gamma-ray emission cited above have not included an important component of inelastic *p*-*p* interaction, the diffractive interaction, nor incorporated the Feynman scaling violation in the non-diffractive inelastic interaction. Another important finding was that these calculations assume an obsolete *p*-*p* non-diffractive inelastic cross-section model taking a constant value of $\sim$ 24 mb for $T_p \gg 10$ GeV. Updating these shortfalls and inaccuracy can change the gamma-ray spectrum from the proton ISM interaction at high energies in the following ways: the diffractive process will add gamma-rays in the highest end of the spectrum; the scaling violation and the up-to-date non-diffractive inelastic cross-section will increase the gamma-ray yield in the GeV to multi-GeV range.

We built a model (model A) representing the latest knowledge on the *p*-*p* inelastic

interaction, and calculated the gamma-ray spectrum due to π^0 produced in the cosmic-ray proton interaction with ISM. The *p*-*p* interaction is simulated separately for the non-diffractive inelastic and for the diffractive processes. The non-diffractive process is calculated by two computer programs: Pythia 6.2 by Sjöstrand et al. (2001) for the proton kinetic energy (T_p) range 512 TeV $\geq T_p \geq$ 52.6 GeV and the model by Stephens & Badhwar (1981) with the parametrization of Blattnig et al. (2000) for 52.6 GeV $\geq T_p >$ 0.488 GeV. The diffractive process is simulated by a program written for this study [2]: it is based on the formulae given in Goulianos (1983), Goulianos (1995), and Goulianos & Montanha (1999). The non-diffractive and diffractive gamma-ray spectra are added according to the cross-section model for model A shown in Columns 2 and 3 of Table 1 and Fig.1a[3].

The gamma-ray spectrum from $pp \rightarrow \pi^0$ will be presented for 3 cosmic proton spectra: power-law spectrum of index 2.0 representing the acceleration site (see, eg., Ellison (2004)); the local interstellar spectrum (referred to as LIS) obtained from the recent primary cosmic proton measurements (see eg. Moskalenko et al. (2002)); and a trial broken power-law spectrum for the Galactic ridge region (index=2.5 and 2.2 for above and below T_p = 20 GeV, respectively).

We also built a reference model, model B, consisting only of the non-diffractive process as all previous models have assumed (Strong et al. 1978; Stephens & Badhwar 1981; Dermer 1986; Stecker 1989). The non-diffractive cross-section assumed in model B approaches a constant value (see Column 4 of Table 1 and Fig.1b) similar to that assumed in the above references. The computer programs for the model A non-diffractive process are used to calculate the model B non-diffractive process except for the Pythia parameters as will be described later in Sec.5.

In the following sections, we will describe how the total inelastic cross-section is broken down in our model A; relate the Feynman scaling hypothesis and numerical simulation codes in a historic perspective; describe how the scaling violation is incorporated in Pythia; introduce our simulation code of the diffractive interaction; and present the gamma-ray spectra obtained with models A and B. We then compare the predictions of model A, Stephens & Badhwar (1981), Strong et al. (2004) and model B with the EGRET gamma-ray spectrum (EGRET Archive) [4]

---

[2]Simulation Program DiffDissocSimulNew.py for model A is available upon request from author.

[3]The first 2 data sets in Figure 1 are from Hagiwara et al. (2002) and the last from the Spires database (see http://www.slac.stanford.edu/spires).

[4]See EGRET archived data at ftp://cossc.gsfc.nasa.gov/compton/data/egret/high_level/combined_data/galactic/counts.g1234_30.g001. We have subtracted all point sources listed in the EGRET 3rd Catalog from

Table 1: p-p Model Cross-Sections and Galactic Proton Spectral Models

T_p	σ(model A)		σ(model B)	Factors for Proton Spectra		
(GeV)	σ(NonDiff)	σ(Diff)	σ(NonDiff)	Ind=2.0	LIS	Trial4GR
4.88E-01	5	0	5	2.05E+03	5.54E+04	3.05E+04
6.90E-01	20	0	20	1.45E+03	4.58E+04	2.01E+04
9.80E-01	23.4	0	23.4	1.02E+03	3.72E+04	1.32E+04
1.38E+00	25	0	24	7.25E+02	2.91E+04	8.75E+03
1.95E+00	27.57	0	24.6	5.13E+02	2.13E+04	5.78E+03
2.76E+00	28.57	0	24.4	3.62E+02	1.49E+04	3.81E+03
3.91E+00	29.27	0	24.1	2.56E+02	9.54E+03	2.51E+03
5.52E+00	29.76	0	23.8	1.81E+02	5.85E+03	1.66E+03
7.81E+00	23.96	6.13	23.4	1.28E+02	3.51E+03	1.09E+03
1.11E+01	23.65	6.68	23	9.05E+01	2.04E+03	7.21E+02
1.56E+01	23.29	7.22	22.6	6.40E+01	1.18E+03	4.75E+02
2.21E+01	22.91	7.76	22	4.53E+01	6.52E+02	3.04E+02
3.13E+01	22.53	8.29	21.6	3.20E+01	3.62E+02	1.81E+02
4.42E+01	22.27	8.72	21.6	2.26E+01	2.01E+02	1.08E+02
6.25E+01	22.23	8.96	21.6	1.60E+01	1.11E+02	6.40E+01
8.84E+01	22.2	9.19	21.6	1.13E+01	6.18E+01	3.81E+01
1.25E+02	22.14	9.43	21.6	8.00E+00	3.43E+01	2.26E+01
1.77E+02	22.14	9.67	21.6	5.66E+00	1.90E+01	1.35E+01
2.50E+02	22.22	9.91	21.6	4.00E+00	1.06E+01	8.00E+00
3.54E+02	22.36	10.15	21.6	2.83E+00	5.86E+00	4.76E+00
5.00E+02	22.58	10.39	21.6	2.00E+00	3.25E+00	2.83E+00
7.07E+02	22.88	10.64	21.6	1.41E+00	1.80E+00	1.68E+00
1.00E+03	23.24	10.88	21.6	1.00E+00	1.00E+00	1.00E+00
1.41E+03	23.67	11.12	21.6	7.09E-01	5.58E-01	5.97E-01
2.00E+03	24.18	11.36	21.6	5.00E-01	3.08E-01	3.54E-01
2.80E+03	24.75	11.6	21.6	3.57E-01	1.74E-01	2.13E-01
4.00E+03	25.4	11.85	21.6	2.50E-01	9.47E-02	1.25E-01
5.66E+03	26.1	12.09	21.6	1.77E-01	5.25E-02	7.43E-02
8.00E+03	26.88	12.33	21.6	1.25E-01	2.92E-02	4.42E-02
1.13E+04	27.72	12.57	21.6	8.85E-02	1.62E-02	2.63E-02
1.60E+04	28.63	12.82	21.6	6.25E-02	8.97E-03	1.56E-02
2.26E+04	29.6	13.06	21.6	4.42E-02	4.98E-03	9.29E-03
3.20E+04	30.64	13.3	21.6	3.13E-02	2.76E-03	5.52E-03
4.53E+04	31.74	13.54	21.6	2.21E-02	1.53E-03	3.29E-03
6.40E+04	32.9	13.79	21.6	1.56E-02	8.50E-04	1.95E-03
9.05E+04	34.12	14.03	21.6	1.11E-02	4.72E-04	1.16E-03
1.28E+05	35.41	14.27	21.6	7.81E-03	2.62E-04	6.91E-04
1.81E+05	36.76	14.51	21.6	5.53E-03	1.45E-04	4.11E-04
2.56E+05	38.18	14.76	21.6	3.91E-03	8.05E-05	2.44E-04
3.62E+05	39.65	15	21.6	2.76E-03	4.47E-05	1.45E-04

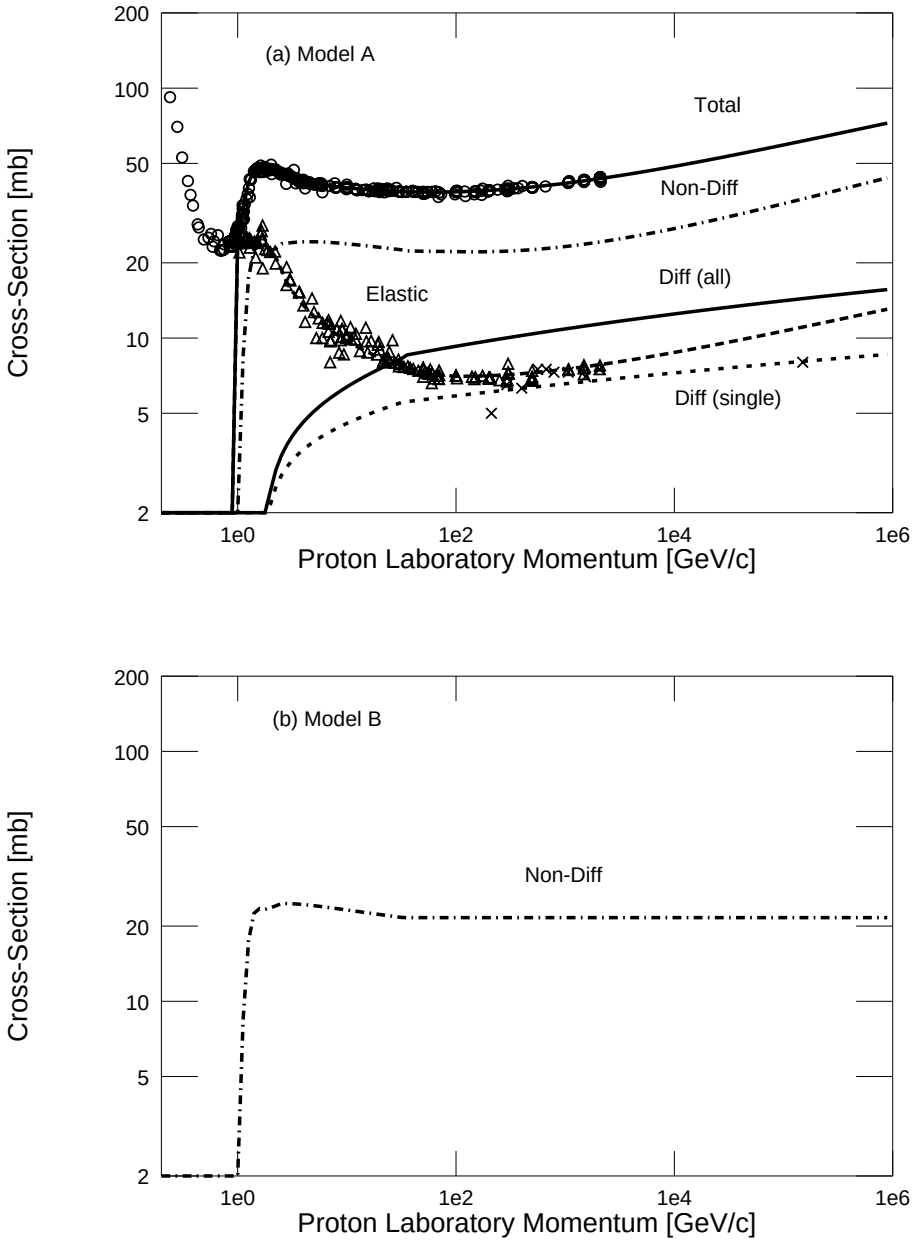

Fig. 1.— The *p*-*p* cross-section models: (a) for model A and (b) for model B. Curves are for the total (*upper solid*), non-diffractive inelastic (*dot-dashed*), elastic (*dashed*), all diffractive (*lower solid*), and single diffractive (*dotted*) processes. Note that model B is made only of non-diffractive inelastic process. Data are for the total (*circles*), elastic (*triangles*), and single diffraction (*crosses*).

Finally discussion on the results, our conclusions, and possible implications on $\bar{p}$, neutrino, e^+, and e^- spectra produced by p-p interactions will be given. Technical details on models A and B will be given in Appendix.

2. Breakdown of the Inelastic Cross-Section

In the present work, the total proton-proton cross-section is broken down to the elastic, non-diffractive inelastic, and diffractive inelastic cross-sections. The total and elastic cross-sections have been measured accurately in the proton kinetic energy range relevant to this study as compilated in Hagiwara et al. (2002)[5] They are plotted as experimental points in Fig.1a together with the cross-sections used in model A. The total inelastic cross-section is, by definition, the difference between the two cross-sections.

Experiments at CERN-ISR established, in mid 1970's, that the total, elastic, and inelastic cross-sections increase with the incident proton energy (Eggert et al. 1975; Baksay et al. 1978; Amaldi et al. 1978). A class of inelastic interaction where the projectile proton and/or the target proton transition to excited states (discrete nucleon resonances and conituum) became known by early 1970's (Alberi & Goggi 1981). This new class of interaction, the diffractive interaction, has been found to grow in cross-section with the incident proton energy (Albrow et al. 1974a,b, 1976; Akimov et al. 1975a,b, 1976). When only one proton transitions to an excited state, the process is called the single diffractive interaction: otherwise the double diffractive interaction. The diffractive process will be explained later in Sec.5.

The early data led to a naive conjecture that the diffractive cross-section increases with the incident proton energy while the non-diffractive inelastic cross section stays constant at $\sim 21 - 24$ mb above ~ 10 GeV. According to recent studies, this conjecture is oversimplification and inaccurate. The increase in the total cross-section is shared by the non-diffractive and diffractive processes as incorporated in the model A cross-sections and shown in Fig.1a (Goulianos 1995; Goulianos & Montanha 1999; Affolder et al. 2001). Fig.1b shows the model B non-diffractive inelastic cross-section: here the diffractive process is completely neglected as has been in all previous predictions on the diffuse Galactic gamma-ray spectrum (Strong et al. 1978; Stephens & Badhwar 1981; Dermer 1986; Stecker 1989; Mori 1997).

---

the data above to make the diffuse gamma-ray spectrum in the Galactic ridge. This point-source subtracted data will be made available in the publication in preparation.

[5]Data on the total and elastic cross-sections are available at http://pdg.lbl.gov/2002/contents_plots.html.

3. Scaling Hypothesis and Simulation of Non-Diffractive Interaction

Scaling hypotheses, or scaling, have been introduced in many branches of physics in many different contexts. Besides the Feynman scaling, there is one more well-known scaling hypothesis for the high energy particle interaction the Bjorken scaling (Bjorken 1969; Perl 1974; Collins & Martin 1984). The hypothesis by Bjorken refers to the lepton-initiated deep inelastic scattering on a nucleon while that by Feynman deals with hadronic interactions. We apply the latter to the $pp \rightarrow \pi^0 X$ cross-section, where X stands for all states reachable from the initial state. The cross-section of this kind is referred to as the (π^0) inclusive cross-section. Historically the Feynman scaling was used to supplement lack of data at higher energies (Strong et al. 1978; Stephens & Badhwar 1981; Dermer 1986; Stecker 1989; Naito & Takahara 1994; Hunter et al. 1997; Mori 1997; Strong et al. 2000; Buesching et al. 2001; Strong et al. 2004). At present, computer-based models are available, such as Pythia (Sjöstrand et al. 2001), where experimental data up to T_p = a few 100 TeV are reproduced. In this section, we will summarize briefly how such a computer program (eg. Pythia) simulates high energy quark-parton interactions and subsequent hadronization.

The scaling hypothesis by Feynman (Feynman 1969) applies to the non-diffractive interaction at high energies ($T_p \gg 10$ GeV). The hypothesis states that cross-sections depend only on the scaling variable $x^*_{||} = 2p^*_{||}/\sqrt{s}$ and p_T at the high energy limit. Here $p^*_{||}$ is the momentum component parallel to the relative motion between the projectile and the target, p_T the perpendicular component, and $\sqrt{s}$ the total energy in the center-of-mass system. This hypothesis has become a powerful tool in extrapolating low energy data to higher energies inaccessible by accelerators (Perl 1974; Collins & Martin 1984).

Feynman proposed the parton model (Feyman 1972) as a physical model realizing the scaling hypothesis. The parton model soon became the quark-parton model and enhanced its predictability. It is, however, the perturbative QCD by Altarelli and Parisi (Altarelli & Parisi 1977) that gave a broader foundation for calculating the absolute cross-section of complex final states. On this basis, Anderson and collaborators started, in late 1970's, the developmental work toward a widely used numerical simulation code for e^+e^- collider experiments, the Lund model (Andersson et al. 1979, 1980; Andersson 1998). Another equally popular simulation code, Herwig, was written a few years later by Webber and Marchesini (Marchesini & Webber 1984; Webber 1984a,b) on a different algorithm known as the Jet Calculus (Konishi et al. 1978, 1979). Pythia (Sjöstrand et al. 2001) is considered as an extension of the Lund model for high energy p-p and p-$\bar{p}$ interactions. Herwig has also been extended to a similar direction (Corcella et al. 2002). We note that simulation codes have been developed for hadron-hadron, hadron-nucleus, neucleus-neucleus, and photon-

nucleus interactions including PHOJET[6]. However they are not as widely used as Pythia and Herwig in simulating high energy p-p interactions. These simulation codes have evolved, cross-checking mutually as well as against experimental data, and built up confidence in the computer-based simulation over 20 years (see, eg., Sjöstrand & Seymour (1999), Mrenna & Richardson (2003) and references therein).

Since both Pythia and Herwig are written on the perturbative QCD, the scaling is violated when a hard parton-parton interaction occurs. However there are many more parton diagrams that violate the Feynman scaling as will be discussed in Section 4. A set of such higher order terms have been added to Pythia recently (Sjöstrand & Skands 2004). We use Pythia without such higher order terms as a reference model (model B) that will approximate, crudely, the Feynman scaling model. We warn, however, that Pythia without the higher order terms (our model B) and the scaling models such as Stephens & Badhwar (1981) and Dermer (1986) give different gamma-ray spectral shapes as has been shown in Fig.3 of Mori (1997).

Table 2 tabulates the computer programs and the cross-section models used in this work.

Several corollary scaling laws have been derived from the quark-parton model. Of them, the best known and relevant to the present paper is the KNO scaling in the particle multiplicity distribution (Koba et al. 1972). According to the KNO scaling, the distribution of the number of secondary particles (eg. π^0 or $\pi^{+/-}$) takes a common shape when re-scaled by the averaged multiplicity of the particle. This scaling law has been used to detect and quantify the scaling violation in the charged particle multiplicity distribution.

4. Scaling Violation in Non-Diffractive Interaction

The two scaling hypotheses of particle physics, the Feynman scaling (Feynman 1969) and the Bjorken scaling (Bjorken 1969), are known to be violated. In literature they are simply referred to as the scale violation. The final states the two hypotheses deal with are both controlled by QCD, but their violation originates from its two different aspects (Perl 1974).

The scaling violation in the p-$\bar{p}$ inclusive cross-section has become evident as the center-of-mass energy reached multi-TeV at CERN-SPS in 1984 (Alpgard et al. 1983; Alner et al. 1984; Breakstone et al. 1984), almost one decade after the violation of the Bjorken scaling had been established. The violation has manifested itself as deviation from the KNO scaling in the multiplicity distribution and excess of jets with large transverse momentuma. The scaling

[6]See R. Engel 1997 at http://www-ik.fzk.de/ẽngel/phojet.html.

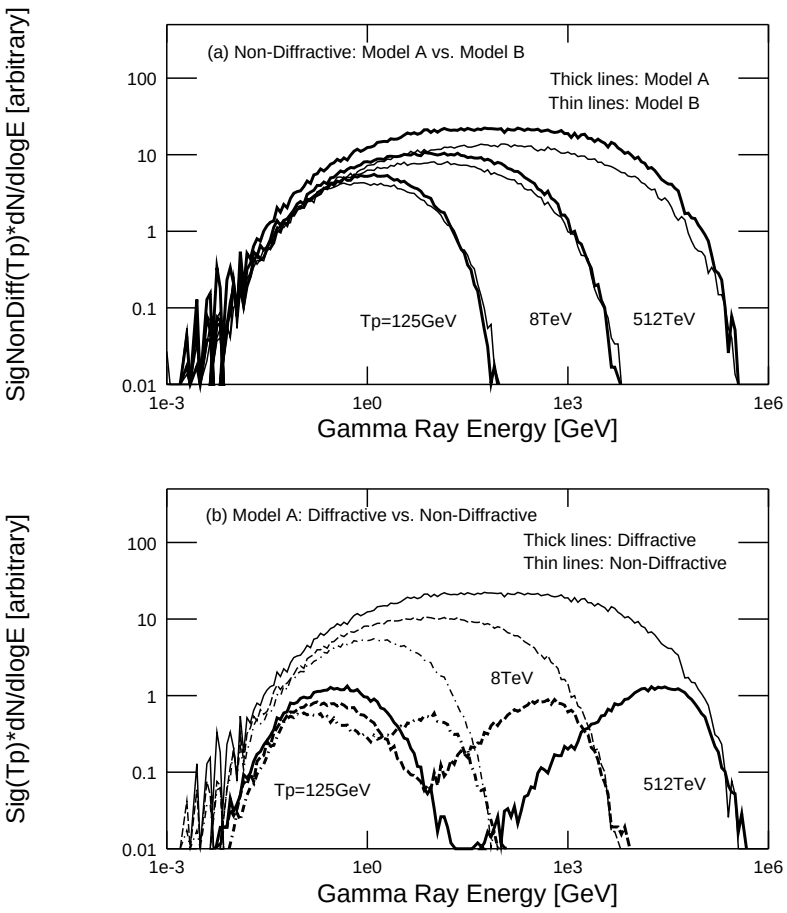

Fig. 2.— Predicted gamma-ray spectra for 3 mono-energetic proton beams: (a) the non-diffractive contribution in model A (*thick lines*) and model B (*thin lines*); and (b) the non-diffractive in model A (*thick lines*) and diffractive in model A (*thin lines*). Proton kinetic energies (T_p) are 512 TeV (solid), 8 TeV (*dashed*), and 125 GeV (*dot-dashed*). Note that model A generates $30 - 80$ % more multi-GeV gamma-rays for $T_p > 100$ GeV.

is now believed to be violated because both the perturbative QCD and the multiple parton interaction introduce new degrees of freedom other than the scaling variable x (Sjöstrand & van Zijl 1987; Sjöstrand & Skands 2004). Such complex processes are best studied by computer simulations: scaling violation due to the perturbative QCD has been included in Pythia from its birth but the multiple parton interaction terms (will be referred to as the higher order terms) have been added recently, eg. in Version 6.2 we use for model A (Sjöstrand et al. 2001).

The CDF collaboration at Fermi Lab. has tuned the parameters controlling the multiple parton interaction in Pythia 6.2 and made the parameter set available as Tune A (Field 2002; Sjöstrand & Skands 2004). We use Pythia 6.2 with this parameter set as the non-diffractive part of model A for $T_p \geq 62.5$ GeV (see Appendix 1 for the parameter setting). We note that we use Pythia 6.1 without the higher order terms in model B: the gamma-ray spectra by the non-diffractive parts of models A and B are compared in Fig.2a. The $\pi^{+/-/0}$ inclusive cross-sections produced by Pythia 6.1 and 6.2 have been verified to agree when they are ran without the higher order terms. The difference in magnitude between models A and B non-diffractive contributions is mostly due to the difference in the two non-diffractive cross-sections (see in Table 1 and Figs.1a and 1b). The scaling violation manifests itself as an increase in the gamma-ray yield and a subtle change in the spectral shape. We defer comparison between the non-diffractive and diffractive parts of model A shown in Fig.2b to Section 5. See Appendix for further details on the Pythia parameter choices.

The scaling violation affects the charged particle multiplicity distribution and violates the KNO scaling: the measured distribution at T_p =21.3 TeV (E_{CM} =200 GeV) by Ansorge et al. (1989) is compared in Fig.3, with model "A All", model A without diffractive interaction, and model B. Since the experiment did not trigger on the single diffractive process, we removed the single diffraction contribution in model "A All". The KNO scaling based on the data taken at $E_{CM} = 30.4$ GeV ($T_p = 490$ GeV) (Breakstone et al. 1984) predicts a skewed normal distribution with mean at 22.3 and mean deviation 11.7, which is close to the model B curve in Fig.3. Important is to note that the model B curve also violates the KNO scaling when compared with the charge multiplicity distribution at $T_p < 50$ GeV (Dao et al. 1973).

The charged multiplicity distribution by Ansorge et al. (1989) shown in Fig.3 is that by the antiproton-proton interaction. In fact high energy ($T_p > 1$ TeV) experimental data to verify our modeling are only available from p-$\bar{p}$ collider experiments at CERN-SPS and Tevatron Collider at Fermi Laboratory. This substitution of p-p by p-$\bar{p}$ is well-founded experimentally up to $E_{CM} = 50$ GeV (Hagiwara et al. 2002) and theoretically for $E_{CM} >$ 50 GeV (see eg. Perl (1974)). The difference between particle- and antiparticle-induced

cross-sections are predicted to diminish asymptotically (Perl 1974; Hagiwara et al. 2002). We have confirmed that the $pp \to \pi$ and $\bar{p}p \to \pi$ cross-sections calculated by Pythia agree within statistical errors at 21.3 TeV.

5. Simulation of the Diffractive Interaction

The diffractive interaction was introduced to particle physics, in 1960, by Good & Walker (1960) as an extension of the theoretical interpretation of deuteron dissociation on the nuclear target by Feinberg & Pomerancuk (1956). In our case the incident proton transitions, after colliding with the target proton, to an excited state with mass M^*, and dissociates to a nucleon and multiple pions. The excited state has the same isospin as the proton. The mass difference, $M^* - M_p$, is much smaller than the total center-of-mass energy, $E_{CM} = \sqrt{s}$. The momentum transfer ($q_{||}$) is small and parallel to the incident momentum (p_p): $q_{||} = (M^{*2} - M_p^2)/2p_p$. Almost the full momentum of the projectile is carried by the excited state. The projectile or target proton goes to an excited state with the same probability: the former is called the projectile diffraction and the latter the target diffraction. The double diffractive interaction refers to the case when both transition to excited states: its cross-section is roughly the same as that of the projectile diffraction.

In mid 1960's, both single and double diffraction phenomena have been observed experimentally (Alberi & Goggi 1981). As has been describe earlier, this interaction has been found to grow in cross-section with the incident energy as shown by the curves labeled as "Diff (all)" and "Diff (single)" in Fig.1a (Albrow et al. 1974a,b, 1976; Akimov et al. 1975a,b, 1976). We note here that the highest energy data point in Fig.1a for the single diffraction come from the collider at CERN where forward-most particles pass through the beam pipe. This leaves some uncertainty in obtaining the angle-integrated cross-section and M^{*2} distribution (see, eg., Donnachie & Landshoff (2004)).

Our program (see footnote 2) first chooses one from the projectile, target and double diffractions. In the program, the single diffraction cross-section is taken from Fig.1 of Goulianos (1995) and the double from Fig.4 of Affolder et al. (2001). We impose a suppression factor for the double diffraction for $T_p < 31$ GeV according to the formula given by Givernaud (1979).

The M^{*2} distribution of the exited state is simulated as a sum of 2 resonances (at 1400 and 1688 MeV) and one continuum tail proportional to $1/M^{*2}$ (Goulianos 1983). Fig.4a shows the M^{*2} distribution our program produces, which approximates that shown in Fig.1 of Akimov et al. (1976) or Fig.25 of Goulianos (1983). The sharp spike at the pion threshold

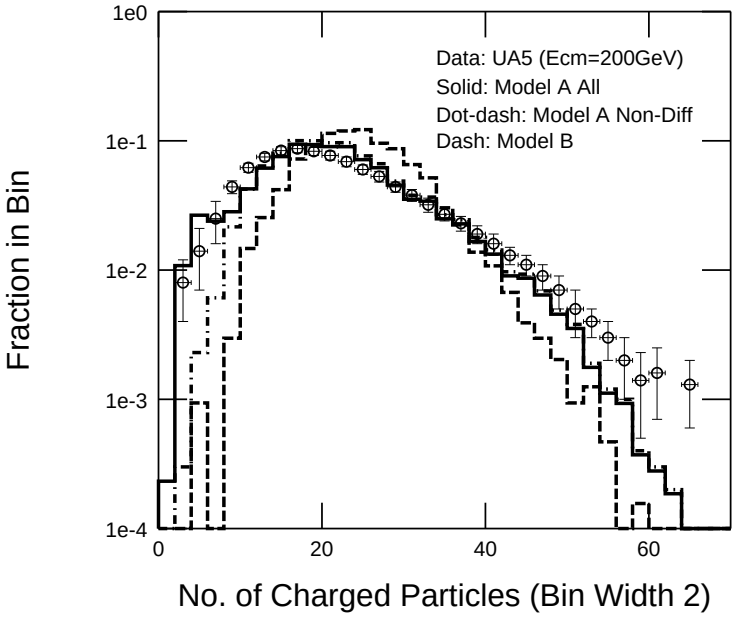

Fig. 3.— Charged particle multiplicity distribution for p-$\bar{p}$ inelastic interaction at $E_{lab} = 21.3$ TeV ($E_{CM} = 200$ GeV). Histograms are: (*solid*) model A non-diffractive + double diffractive, (*dot-dashed*) model A non-diffractive, and (*dashed*) model B. Data are from Ansorge et al. (1989).

($M^{*2} \sim 1.2$ GeV) is an artifact in the program and does not affect the results presented here.

For a M^* chosen, a charge multiplicity is selected from the normal distribution with average of $n_0 = 2.0\sqrt{M^* - M_p}$ (masses in GeV) and rms of $n_0/2$ (Cool et al. 1982; Goulianos 1983). We then choose a π^0 multiplicity with average of $n_0/2$ and rms of $n_0/4$. Fig.4b shows the charged multiplicity distribution for the single diffraction of $T_p = 21.3$ TeV or $E_{CM} = 200$ GeV. This can be compared with that for the non-diffractive process at the same energy shown in Fig.3.

The charged multiplicity is divided between π^+ and π^- under the charge conservation: for an odd charged multiplicity we make one more π^+ than π^-; for an even charged multiplicity, we make an equal number of π^+ and π^-, implying the associated baryon is proton. Available energy, $M^* - M_p - nM_\pi$, will be divided randomly among the pions. Note that the kinetic energy going to the nucleon can be neglected because $M_p \gg M_\pi$ in the CM system of M^*.

Finally the momentum of the excited state is calculated on the basis of energy-momentum conservation: its distribution peaks sharply toward the momentum the projectile (see Fig.4c), in this case, 21.3 TeV/c in the laboratory frame. The pion momenta in the CM system of M^* are then transformed to the laboratory frame, and the neutral pions among them are forced to decay to gamma-rays.

Gamma-ray spectra produced by our diffractive interaction simulator are compared with those by the model A non-diffractive process in Fig.2b. Note that the projectile diffraction contributes in a narrow energy band at around one-tenth of T_p while the target diffraction piles up in a narrow energy band around 100 MeV almost independently of the incident proton energy.

We note that the diffractive dissociation has also been implemented in Pythia 6.1/6.2 (Sjöstrand et al. 2001) and in PHOJET (see footnote 6). The particle interaction modeling of our model A is similar to that used in Pythia: in fact the total charge multiplicity distribution including the double diffraction by Pythia 6.2 with the higher order terms is similar to that of model A shown in Fig.3. Detailed comparison on the difference between the diffractive parts of Pythia and PHOJET is given in a review by Guillaud & Sobol (2004). We note that the diffractive parts of Pythia and PHOJET are optimized in combination with their respective non-diffractive counter parts.

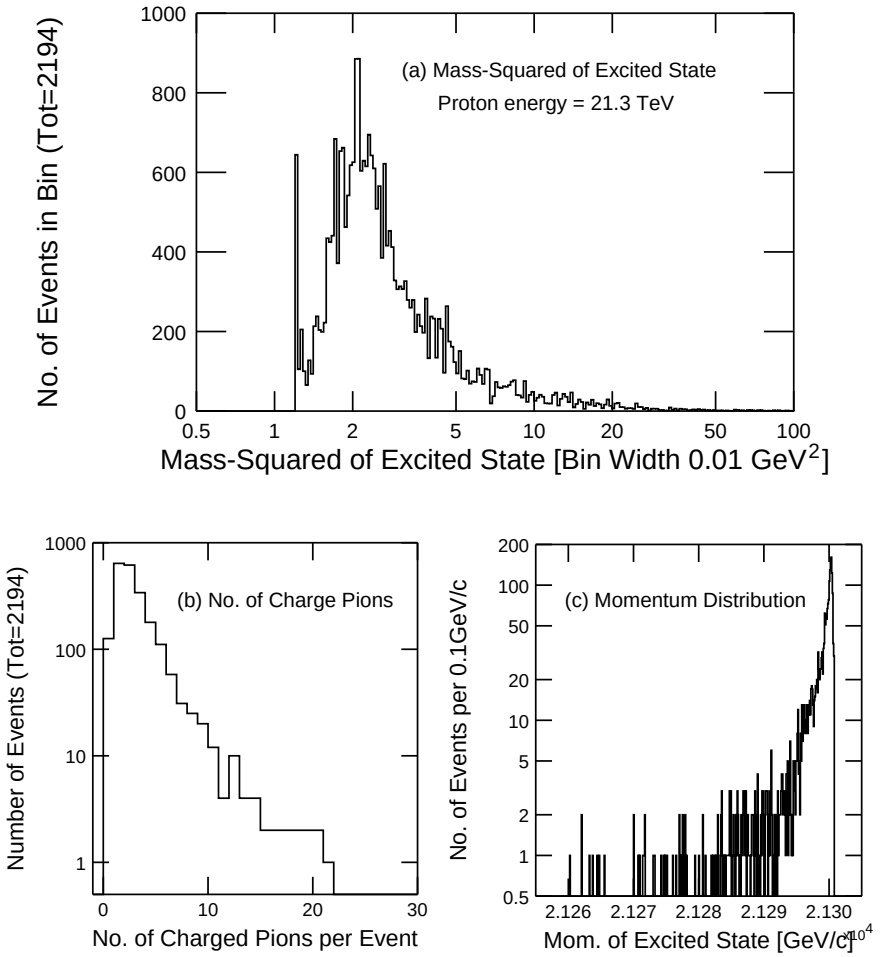

Fig. 4.— Distributions of 3 quantities in projectile diffraction events at $T_p = 21.3$ TeV generated by DiffDissocSimNew.py: (a) M^{*2} mass, (b) charged pion multiplicity, and (c) laboratory momentum of M^*. Note that a sharp spike in (a) at mass-squared 1.2 GeV^2 is an artifact.

6. Gamma-Ray Spectra for Model Spectra of Galactic Protons

Before proceeding to calculate the gamma-ray spectra produced by protons with continuum spectra, we have summed the π^0 yields from the non-diffractive and diffractive interactions to compare with the experimental data listed in Dermer (1986). Fig.5 shows the inclusive π^0 cross-section or, equivalently, the average multiplicity of π^0 per p-p interaction multiplied by the cross-sections for $pp(\bar{p}p)$ collisions: the solid line, labeled as model "A All", is the sum of the non-diffractive and double diffractive contributions; the dashed line, labeled as model B, represents the non-diffractive contribution without the multiple parton interaction terms. We note that contribution of the diffractive process, model A diff, is small in the multiplicity, just as in the charged multiplicity shown in Fig.3. Model A reproduces the measured π^0 multiplicity quite well above the resonance region ($T_p > 3$ GeV). We also note that the scaling model of Dermer (1986) as well as our model B reproduce the data well.

To the accuracy needed for the present study, continuum spectra of protons can be approximated by a sum of a series of mono-energetic proton beams. We choose a geometrical series of $T_p = 1000.0 \times 2^{(N-22)/2}$ GeV where $N = 0 - 40$. Each proton energy bin covers from $2^{-0.25}T_p$ to $2^{0.25}T_p$. The gamma-ray spectra for mono-energetic protons of kinetic energies T_p listed in Column 1 of Table 1 are weighted by the appropriate p-p cross-sections for the energy given in Columns 2-4. Figs.2a and 2b show such samples for 3 T_p's for models A and B, and for the non-diffractive and diffractive interactions. The cross-section-weighted gamma-ray spectra for mono-energetic protons of T_p is then multiplied with a proton spectrum factor of the three listed in Column 5-7. By summing over all T_p's we obtain the gamma-ray spectrum for the proton spectrum. We note here that the sum over a geometrical series of proton kinetic energies (T_p) makes the gamma-ray spectrum corresponding to a proton spectrum with power-law index 1.0. The 3 proton spectral factors in Table 1 are accordingly adjusted and mutually normized to 1.0 at $T_p = 1$ TeV: they will be normalized differently, as will be described below, when the gamma-ray fluxes are obtained.

Among many model spectra proposed for the Galactic protons, we have chosen the power-law spectrum of index 2.0, the local interstellar spectrum, and a trial spectrum for the Galactic ridge region. We give short description on them below.

Ind2: Power-law spectrum with index 2.0 representing the proton spectrum at acceleration sites (eg. Ellison (2004)).

LIS: Local Interstellar Spectrum (LIS) defined as the spectrum just outside of the solar system. It can be obtained by removing the solar modulation effect from cosmic ray spectra measured around the Earth. Our LIS has been taken from the solid curve

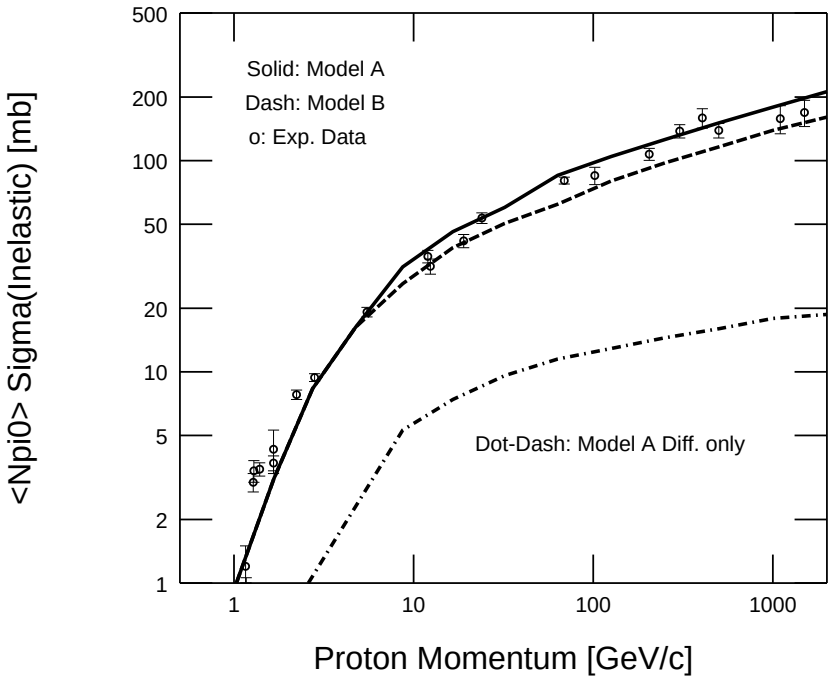

Fig. 5.— Averaged neutral pion multiplicity for the p-p and p-$\bar{p}$ inelastic interaction. Curves are for model "A All" (*solid*), model B (*dashed*), and model A diffractive (*dot-dashed*). Data are from Table 1 of Dermer (1986).

in Fig.4 of Moskalenko et al. (2002) that has been obtained as a result of fitting GALPROP to various observational data. It takes a power-law spectrum with index 2.7 for $T_p > 15$ GeV .

Trial4GR: A broken power-law spectrum with indices 2.5 ($T_p > 20$ GeV) and 2.2 ($T_p < 20$ GeV). Considering various uncertainties in the source spectra, propagation, and possible reacceleration of protons and electrons, this trial spectrum remains to be a possibility in the Galactic ridge region.

The total gamma-ray spectra for Ind2, LIS and Trial4GR are presented after multiplying with E_γ^2 for models A and B in Figs.6a, 6b and 6c. We note that model A gives harder gamma-ray spectra than model B for all 3 proton spectra for $E_\gamma > 1$ GeV (Fig.6): the asymptotic power-law indices for model A/model B are 1.96/2.03 for Ind2, 2.65/2.71 for LIS and 2.47/2.53 for Trial4GR. It is to be noted that the model A gamma-ray spectra are harder than those of incident protons by index ~ 0.05.

7. Comparison with EGRET Galactic Ridge Spectrum

The EGRET count and exposure maps for the observation period 1-4 have been downloaded from the EGRET archive (see footnote 3). All point sources listed in the EGRET 3rd Catalog (Hartman 1999) are then removed using the point-spread function of EGRET for each energy band and for the power-law index of each point source listed in the catalog. The flux between 100 MeV and 10 GeV has been constrained to that of each point source listed in the EGRET 3rd Catalog. The point-source-subtracted count map is then divided by the corresponding exposure map to make the intensity map. The intensity between the Galactic latitude ± 6.0 deg. and Galactic longitude ± 30.0 deg has been summed and normalized to a unit solid angle to become our EGRET Galactic ridge spectrum used in this work. The point-source-subtracted intensity map has been checked to be consistent with the similar map given in Strong et al. (2000). The intensity is then divided by the bin width and multiplied by E_{bin}^2, or the mid-energy squared. The results are given in the 4th column of Table 3.

A second EGRET spectrum has been calculated in the same manner as above except that the point-source-subtracted count map is processed further to deconvolve the point spread function (PSF): energy dependency of the PSF used in the deconvolution has been derived assuming a power-law incident gamma-ray (index 2.1). Details will be described in a separate publication (T. Kamae et al. 2005, in preparation). The deconvolution removes artifacts introduced by the broad EGRET PSF, in particular, for $E_\gamma < 150$ MeV and allows

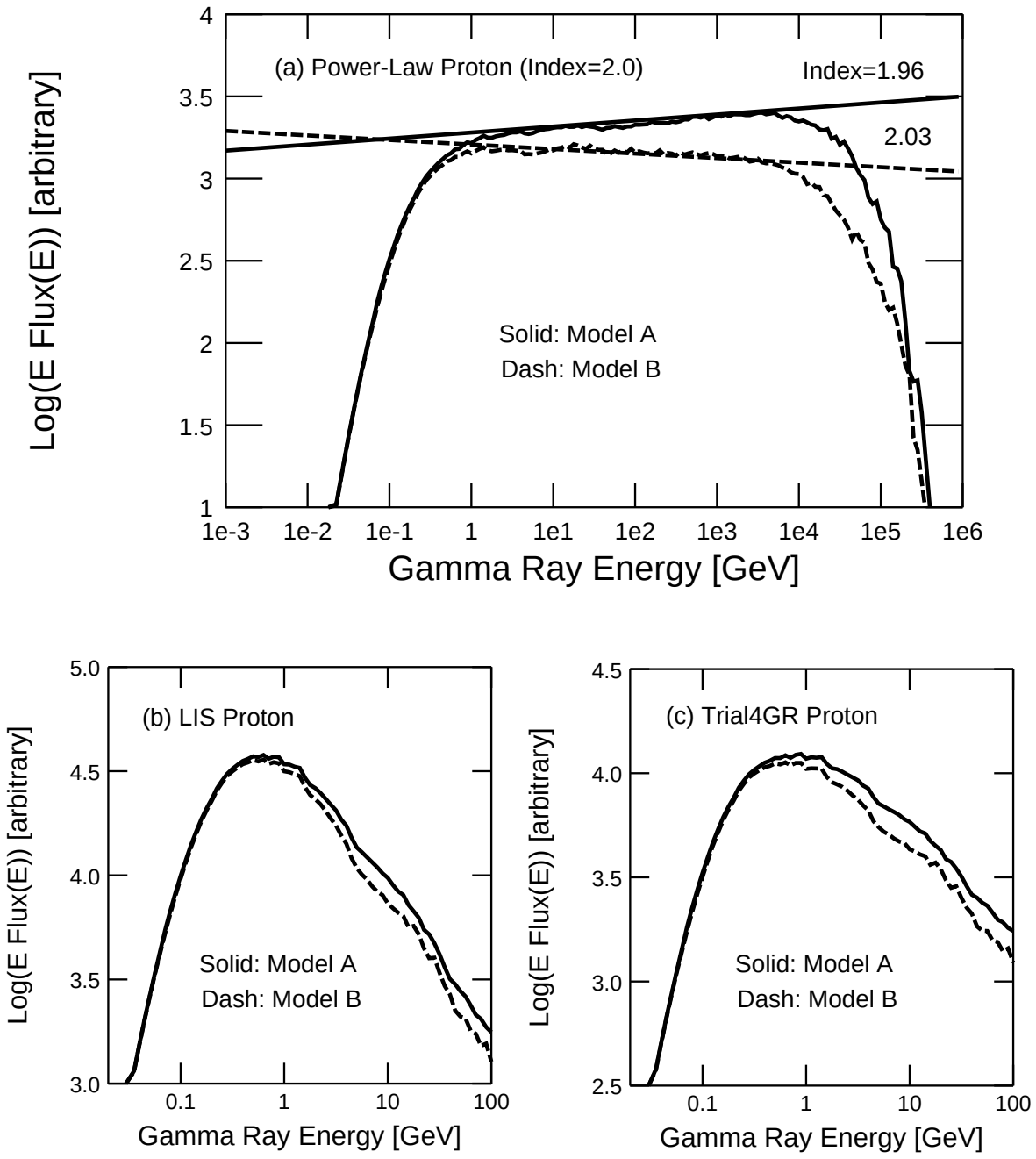

Fig. 6.— Gamma-ray spectra predicted for the 3 proton spectra between 0.488 GeV $< T_p <$ 512 TeV: (a) power-law with index=2.0, (b) LIS, and (c) Trial4GR. Curves are for model A (*solid*) and model B (*dashed*). Asymptotic power-law indices of gamma-ray spectra are: 1.96/2.03 (Index=2 model A/model B), 2.65/2.71 (LIS model A/model B), and 2.47/2.53 (Trial4GR Model A/Model B).

us to compare the observed spectrum and model predictions directly. Thus obtained EGRET Galactic ridge spectrum (referred to as "deconvolved") is given in the 5th column of Table 3.

The numbers of gamma-rays in our Galactic ridge region before the deconvolution are: 2768, 7700, 18656, 26784, 50081, 27469, 22601, 10971, 4217, and 1235 for the 10 EGRET energy bands in the ascending order in energy. The statistical uncertainty (fwhm) is 4% or better except for the lowest and highest energy bands. However, possible systematic error associated with the EGRET spectrum is hard to assess: we assume it to be ±15% as has been done in Strong et al. (2004).

When steep spectra (eg. power-law index $\sim 2.0-3.0$) are histogrammed in wide energy bins as had been done in the EGRET data analysis, some systematic bias may be introduced. We studied this bias by binning model A predictions for LIS and Trial4GR into the EGRET bins and multiplying with the mid-energy of the bins. The coarsely-binned data tend to give higher values of $E_\gamma^2 \times Flux(\gamma)(= E_\gamma \times Flux(E_\gamma))$ but the difference is only 5-10% and negligible in the accuracy of the present work.

We proceed to calculate the E_γ^2-weighted gamma-ray flux (equivalent to $E_\gamma^2 \times Flux(\gamma)$) for EGRET, model A with LIS, model B with LIS, the GALPROP result obtained with the conventional parameter setting where the cosmic-ray proton spectrum becomes LIS (Strong et al. 2004), and the result given in Stephens & Badhwar (1981). We note that the GALPROP model described in Strong et al. (2000), Moskalenko et al. (2002), and Strong et al. (2004) with the conventional parameter setting give similar gamma-ray spectrum. We refer to the one in Strong et al. (2004) because it is produced with the current (C++) version of GALPROP.

As has been stated in Sec.1, the gamma-ray spectrum of EGRET should be analyzed including the contributions from bremsstrhlung and inverse-Compton. However, the GeV Excess was first noted by comparing the shape of E_γ^2-weighted EGRET spectrum with that obtained on the π^0 inclusive cross-section based on the scaling hypothesis. Because of this history, we focus on the spectral shape in Fig.7 and normalize the 4 model E_γ^2-weighted gamma-ray spectra in the energy range $E_\gamma < 300$ MeV where the $\pi^0 \rightarrow \gamma$ spectrum becomes insensitive to the incident proton spectrum. The EGRET data has been normalized so that the average of the $150-300$ MeV and $300-500$ MeV bins to agree with the model A prediction. We note that the proton spectrum assumed in Stephens & Badhwar (1981) has a power-law index of 2.75 and a break at $T_p = 7$ GeV.

Model A with the LIS spectrum predicts a broad peak at around ∼0.8 GeV for gamma-rays of π^0 origin: its spectral shape is closest to that of the EGRET ridge data among

Table 2: Models of p-p interactions and Cross-Sections

	Non-Diffractive		Diffractive
Proton K.E. (T_p)	Model A	Model B	Model A
Cross-Section Models			
0.410GeV−609TeV	Table 1 col. 2 Fig.1a Non-Diff	Table 1 col.4 Fig.1b Non-Diff	Table 1 col. 3 Fig.1a Diff(all)
Interaction Models			
0.410−52.6 GeV	Stephens & Badhwar (1981) Eqs.23/24 and eq.32 of and Blattnig et al. (2000)		DiffDissocSimNew.py[a] T. Kamae(2004, per. comm.)[a]
52.6GeV−609TeV	Pythia6.2 (Higher order) ("Tune A")	Pythia6.1 (No higher order)	T. Kamae(2004, pers. comm.)[a]

[a]Simulation program DiffDissocSimulNew.py for model A is available upon request from author.

Table 3: EGRET Spectra of Galactic Ridge

EGRET Energy Bins			$log_{10}(E_\gamma^2 Intensity)$	
E_{min}	E_{max}	$Log(E_{center})$	Intensity Map	Deconv. Int. Map
(MeV)	(MeV)	(GeV)	(GeV/cm^2/sr/s)	(GeV/cm^2/sr/s)
30	50	-1.411	-4.7969	-4.6875
50	70	-1.227	-4.8109	-4.7406
70	100	-1.077	-4.7140	-4.6631
100	150	-0.911	-4.6005	-4.5674
150	300	-0.673	-4.4144	-4.3987
300	500	-0.411	-4.3384	-4.3313
500	1000	-0.150	-4.2367	-4.2367
1000	2000	0.150	-4.1924	-4.1924
2000	4000	0.451	-4.2538	-4.2538
4000	10000	0.801	-4.4153	-4.4153

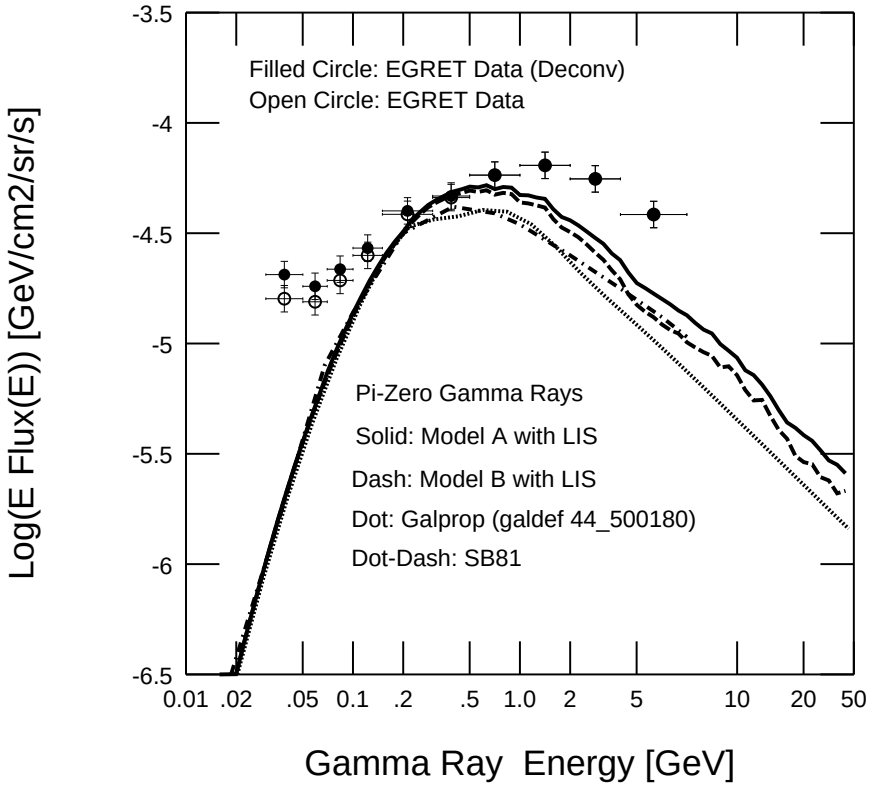

Fig. 7.— Model π^0 gamma-ray spectra and the EGRET data: The filled circles are for the PSF deconvolved EGRET spectrum; and the open circles are for the EGRET spectrum, both for the Galactic Ridge ($-6 < b < 6$ deg, $-30 < \ell < 30$ deg). Model curves are for model A with LIS (*solid*), model B with LIS (*dashed*), Stephens & Badhwar (1981)(*dot-dashed*), and GALPROP with the conventional cosmic ray spectra (Strong et al. 2004)(*dotted*). Model spectra are mutually normalized in $E_\gamma < 300$ MeV. The EGRET data (*open circle*) are normalized to the model A with LIS in $150 < E_\gamma < 500$ MeV.

the four shown in Fig.7. The proton spectrum in the Galactic ridge region is considered to lie between that of the source speculated to be close to that of power-law with index ~ 2.0 (Ellison 2004) and that observed at ~ 8.5kpc away, a power-law spectrum with index ~ 2.7. When we compare model B with LIS (*dashed*) with Strong et al. (2004) (*dotted*) and Stephens & Badhwar (1981)(*dot-dashed*), we note that model B produces more higher energy gamma-rays than the others. This is interpreted as due to the fact that Pythia without the higher order terms over-produces π^0 in the forward-most phase-space region or the highest energy region as noted by Mori (1997). We note that the asymptotic power-law index of model B is similar to that of Strong et al. (2004).

As the final step of analysis, we combine the model A prediction with the bremsstrahlung and inverse-Compton spectra predicted by GALPROP with the conventional cosmic ray spectra (the parameter "galdef 44_500180" in Strong et al. (2004)). Here we normalize the model A $\pi^0 \rightarrow \gamma$-ray spectra (with LIS and Trial4GR) to π^0 gamma-ray spectrum of this GALPROP model in the energy region $E_\gamma < 300$ MeV as has been done in Fig.7. Since the contributions by pion decay, bremsstrahlung, and inverse Compton are mutually fixed within the GALPROP model, we add the model A (Trial4GR and LIS), the GALPROP bremsstrahlung, and the GALPROP inverse Compton to obtain the spectra labeled as "model A with Trial4GR" (*solid curve*) and "model A with LIS" (*dashed curve*). We note that the normalization to the EGRET data relative to the 3 models is still unconstrained and our focus should be on the spectral shape.

In Fig.8 we note that the peak energies and the widths of the two model A spectra (LIS and Trial4GR) are closer to those of the EGRET data than those of the GALPROP with the conventional cosmic-ray spectrum (galdef 44_500180): the discrepancy in the GeV region or "GeV Excess" is reduced to about 50 % if we compare model A (LIS) and the GALPROP spectrum. When compared with the spectra in Fig.7, the addition of the bremsstrahlung contribution shifts the peaks in $E_\gamma^2 F(\gamma)$ to lower energies. The EGRET spectrum deconvolved of the point spread function improves the agreement between the data and the models slightly in the lower slope of the gamma-ray spectrum. The proton spectrum Trial4GR combined with model A (Fig.8, *solid curve*) produces a $E_\gamma^2 F(\gamma)$ spectrum consistent with that of the EGRET data in the GeV range.

The higher π^0 yield in model A relative to model B implies higher anti-proton yield. Our study (T. Kamae et al. 2005, in preparation) shows that Pythia 6.2 with the higher order terms, with the model A cross-section, and with the LIS proton spectrum produces $\sim 1.5 - 2.0$ times more secondary anti-protons than that without the higher order terms, with the model B cross-section, and with the LIS proton spectrum, for $E(\bar{p}) = 1 - 20$ GeV (see Fig.9). Several comments are in order. The non-diffractive inelastic process is expected

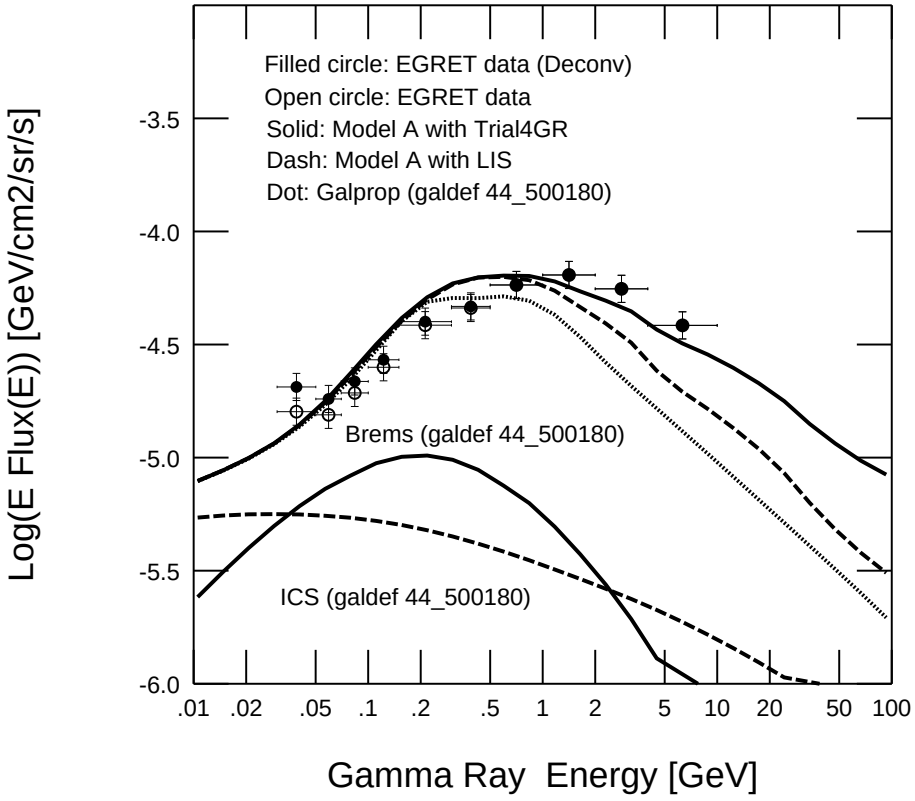

Fig. 8.— Model gamma-ray spectra including the contributions from bremsstrahlung and inverse-Compton and the EGRET data: Data labels are same as in Fig.7. Model curves are :(Brems) bremsstrahlung contribution; (ICS) inverse-Compton contribution, of GALPROP with parameters galdef 44_500180 in Strong et al. (2004). Other curves are: model A (Trial4GR)+Brems+ICS (*solid*); model A (LIS)+Brems+ICS (*dashed*); π^0+Brems+ICS by GALPROP with galdef 44_500180 (Strong et al. 2004) (*dotted*).

to produce $\bar{p}$ even for $T_p < 62.5$ GeV. However our low energy model based on Stephens & Badhwar (1981) and Blattnig et al. (2000) has not been implemented with the $pp \rightarrow \bar{p}$ inclusive process. Hence we have used Pythia 6.2 with the higher order terms and Pythia 6.1 to $T_p = 10$ GeV for models A and B, respectively, to obtain the $\bar{p}$ yield shown in Fig.9.

8. Conclusion and Future Prospect

We conclude on the analyses presented here that an accurate modeling of the p-p interaction (model A) with the diffractive process and the Feynman scaling violation makes the gamma-ray spectrum harder and produces 30−80% more gamma-rays (Figs.6, 7, and 8) than previous predictions (Strong et al. 1978; Stephens & Badhwar 1981; Dermer 1986; Stecker 1989; Mori 1997) for incident protons with $T_p > 100$ GeV. Combination of the two can explain ~ 50 % of the "GeV Excess" in the EGRET Galactic ridge spectrum within the conventional cosmic proton and electron spectra as shown in Fig.8. The above statement is only relative to other $pp \rightarrow \pi^0$ production models: the absolute prediction of the Galactic ridge gamma-ray spectrum is contingent on the absolute normalization, or the absolute cosmic ray fluxes, the absolute ISM density, and the absolute radiation field density. As far as the gamma-ray spectral shape is concerned, the remaining discrepancy (50%) requires some modification to the conventional cosmic ray spectra: one possibility is to assume the proton spectrum in the Galactic ridge to be a little harder than that of the solar neighborhood, eg. ~ 2.5 in power-law index as Trail4GR in Fig.8.

We have compared model A critically with data from accelerator experiments (Figs.1a, 3, 4, and 5) and confirmed that important aspects of experimental data are reproduced much better by model A than model B which crudely reflects the Feynman scaling hypothesis. We believe that all future cosmic p-p interaction models must include the diffractive process and incorporate the scaling violation.

Model A with LIS predicts the $\bar{p}$ flux to be higher by a factor of $\sim 1.5 - 2$ relative to model B. We will compare the above prediction with the recent measurements on the $\bar{p}$ flux (Orito et al. 2000; Asaoka et al. 2002; Basini et al. 1999; Boezio et al. 2001) and the prediction by Moskalenko et al. (2002) in a separate publication (T. Kamae et al. 2005, in preparation).

In this work, we have neglected contributions of α particles and helium atoms/ions to the gamma-ray spectrum. We note that the abundance of helium atoms/ions is about 7% of hydgrogen atoms/ions and so is the α to p ratio. The spectral index of α particles is known to be lower by about 0.1 (see eg., Mori (1997); Schlickeiser (2002)). Since there

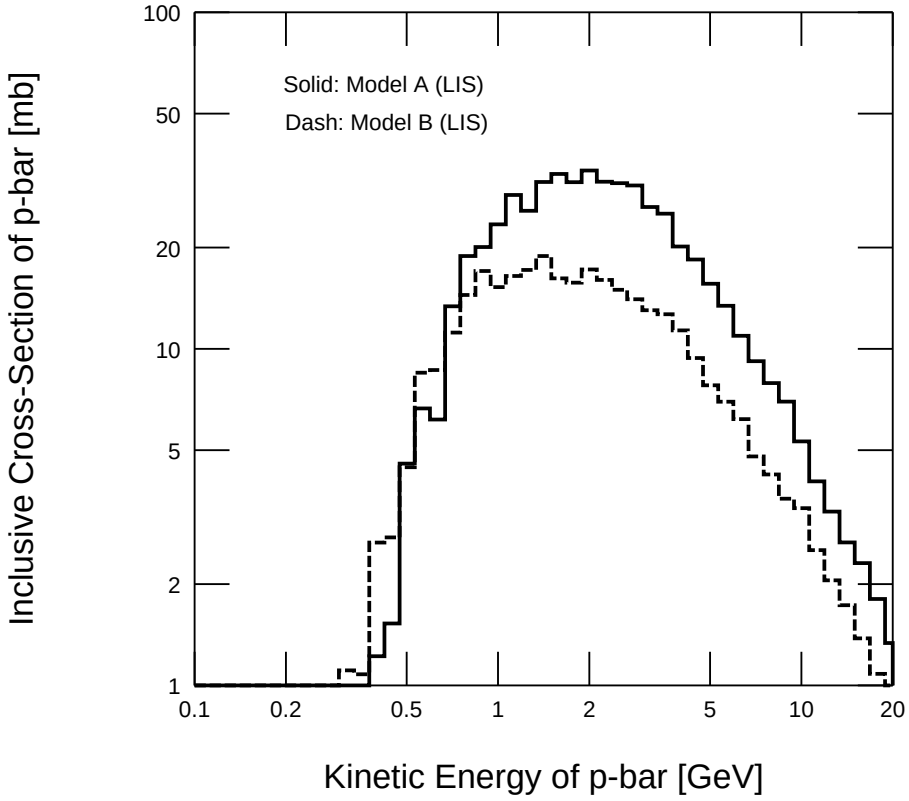

Fig. 9.— Anti-protons spectra predicted for the local cosmic ray proton spectrum (LIS) by model A (*solid curve*) and model B (*dashed*). The bin width is 5 % of proton kinetic energy. The low energy non-diffractive model of Stephens & Badhwar (1981) has been replaced by Pythia for this calculation (see text).

are no measurement on the π^0 inclusive cross-section for pHe, αp, and αHe interactions at high energies, we refer to an estimate on possible deviation from that of p-p. We take the results obtained on pd and p-p interactions by Akimov et al. (1976). From the reference, we learn that: the $(\sigma_T(pd)/\sigma_T(pp))^2$ remains constant over the incident momentum range of the experiment; and the coherent factor in the diffractive process is less than 10%. Since the coherent factor decreases rapidly as the momentum transfer increases, we expect it to be much smaller than 10 % for the non-diffractive process. By inference we conclude that the gamma-ray spectra produced by pHe, αp, and αHe interactions can safely be represented by those by p-p interactions as has been done in this work.

The findings of this work make the following interesting predictions on the spectra of other cosmic ray particles (T. Kamae et al. 2005, in preparation):

- The diffractive interaction and scaling violation (model A) nearly double the TeV gamma-ray yield from interaction of power-law protons with index=2.0, compared to that predicted with model B or our approximation to the scaling model (see Fig.6a). We also expect all decay products of charged pions (e^+, e^-, ν_e, $\bar{\nu_e}$, ν_μ, and $\bar{\nu_\mu}$) to increase by a similar proportion near the highest end of their spectra.

- Combination of the inherently low multiplicity of the diffractive process and the charge conservation predicts ~ 1.5 times as many π^+ as π^- for $T_p = 512$ TeV protons as shown in Fig.10. We hence expect e^+/e^- and $\nu_e/\bar{\nu_e}$ to increase near the highest end of their spectra where the diffractive process contributes most. We note that possible increase of e^+ relative to e^- has been reported in the cosmic e^+ spectrum above 5 GeV. (Coutu et al. 1999).

One of the authors (Kamae) would like to acknowledge valuable discussions with Igor Moskalenko, Andy Strong and Dino Goulianos. Moskalenko informed him of the possible excess observed in the e^+ spectrum (Coutu et al. 1999). Moskalenko and Strong kindly made the GALPROP program and galdef parameter files available to him and answered many questions about the program. Goulianos directed him to several references. The authors acknowledge the referee for informing them of PHOJET, making valuable suggestions to improve the description, and correcting errors. T. Mizuno, I. Moskalenko and K. Goulianos kindly read an early version of the manuscript and helped to make this paper readable both for astrophysicists and particle physicists. The authors gratefully acknowledge advice and assistance given by D. Elwe, J. Chiang, S. Digel, I. Grenier, P. Kunz, G. Madejski, H. Tajima P. Nolan, R. Hartman, S. Hunter, M. Mori, J. Ormes, F. Stecker, D. Thompson, M. Asai, N. Graf and Y. Shimizu.

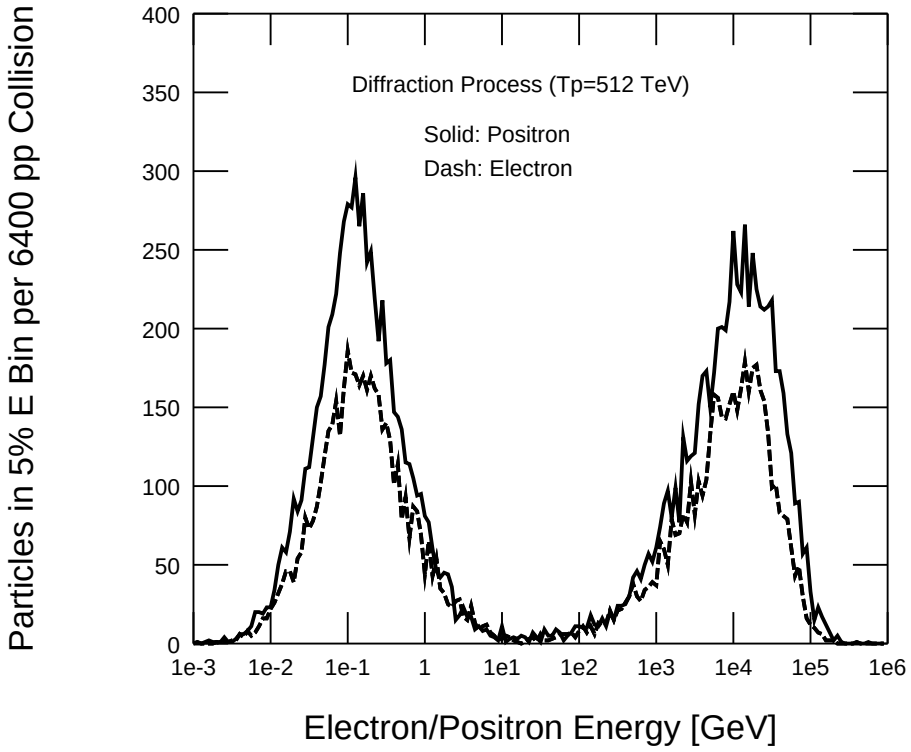

Fig. 10.— Spectra of electrons (*dashed curve*) and positrons (*solid curve*) produced in 6400 diffractive interactions by protons with $T_p = 512$ TeV.

A. Parameter Settings of Pythia for Models A and B

Pythia has been used to calculate the $\pi^0 \rightarrow \gamma$ inclusive cross-section for $T_p \geq 62.5$ GeV. The following parameter settings of Pythia have been used for models A and B. The gamma-ray spectra generated by model A are shown in Fig.11 for several monoenergetic proton beams.

- Model A: Pythia 6.2 with the following parameter setting (Sjöstrand et al. 2001; Field 2002).
  - Setup for the multiple interaction "CDF tune A":
    MSTP(81) = 1
    PARP(82) = 2.0
    PARP(89) = 1800.0
    PARP(90) = 0.25
    MSTP(82) = 4
    PARP(83) = 0.5
    PARP(84) = 0.4
    PARP(85) = 0.9
    PARP(86) = 0.95
    PARP(67) = 4.0
  - The default setup for *p*-*p* interaction by setting MSEL in COMMON/PYSUBS/ to 1: MSEL=1
  - Force charged pions, charged kaons, K-long's and muons to decay instantly:
    KCPI = PYCOMP(211)
    MDCY(KCPI,1) = 1
    KCK = PYCOMP(321)
    MDCY(KCK,1) = 1
    KCKL = PYCOMP(130)
    MDCY(KCKL,1) = 1
    KCMU = PYCOMP(13)
    MDCY(KCMU,1) = 1
- Model B: Pythia6.1 with the following parameter setting (Sjöstrand et al. 2001).
  - The default setup for *p*-*p* interaction by setting MSEL in COMMON/PYSUBS/ to 1: MSEL=1

- Force charged pions, charged kaons, K-long's and muons to decay instantly:
  KCPI = PYCOMP(211)
  MDCY(KCPI,1) = 1
  KCK = PYCOMP(321)
  MDCY(KCK,1) = 1
  KCKL = PYCOMP(130)
  MDCY(KCKL,1) = 1
  KCMU = PYCOMP(13)
  MDCY(KCMU,1) = 1

B. Low Energy Formulae for the Non-Diffractive Process for Models A and B

The cross-sectional formulae of Stephens & Badhwar (1981) parametrized by Blattnig et al. (2000) have been used to calculate the $\pi^0 \rightarrow \gamma$ inclusive cross-section for $T_p \leq 44.2$ GeV. Blattnig et al. (2000) gives two different parameterizations. One (No.1 below) reproduces the overall π^0 momentum distribution better but under-predicts higher energy π^0 yield in the p-p center-of-mass system. The other (No.2 below) gives a poorer overall agreement and over-predicts higher energy π^0 yield. We have mixed the two parameterizations so that the E_γ^2-weighted gamma-ray spectrum connects smoothly to that by Pythia at $T_p = 62.5$ GeV.

- Parameterization No.1 of Stephens & Badhwar (1981):
  - $T_p = 0.3 - 2.0$ GeV: Eq. 23 of Blattnig et al. (2000).
  - $T_p = 2.0 - 44.2$ GeV: Eq. 24 of Blattnig et al. (2000).
- Parameterization No.2 of Stephens & Badhwar (1981):
  - $T_p = 0.3 - 44.2$ GeV: Eq. 32 of Blattnig et al. (2000).
- Mix of Param-1 and Param-2 used in models A and B:
  - $\sigma(\pi^0) = (1.0 - R)\sigma(\pi^0$:Param-1) $+ R\sigma(\pi^0$:Param-2)
    where the ratio R has been set to 0.15 to make the gamma-ray spectrum smoothly transform from $T_p = 44.2$ GeV by the mixed formula to $T_p = 62.5$ GeV by Pythia.

The gamma-ray spectra generated by the above Mix of Param-1 and Param-2 are shown in Fig.11 for several monoenergetic proton beams.

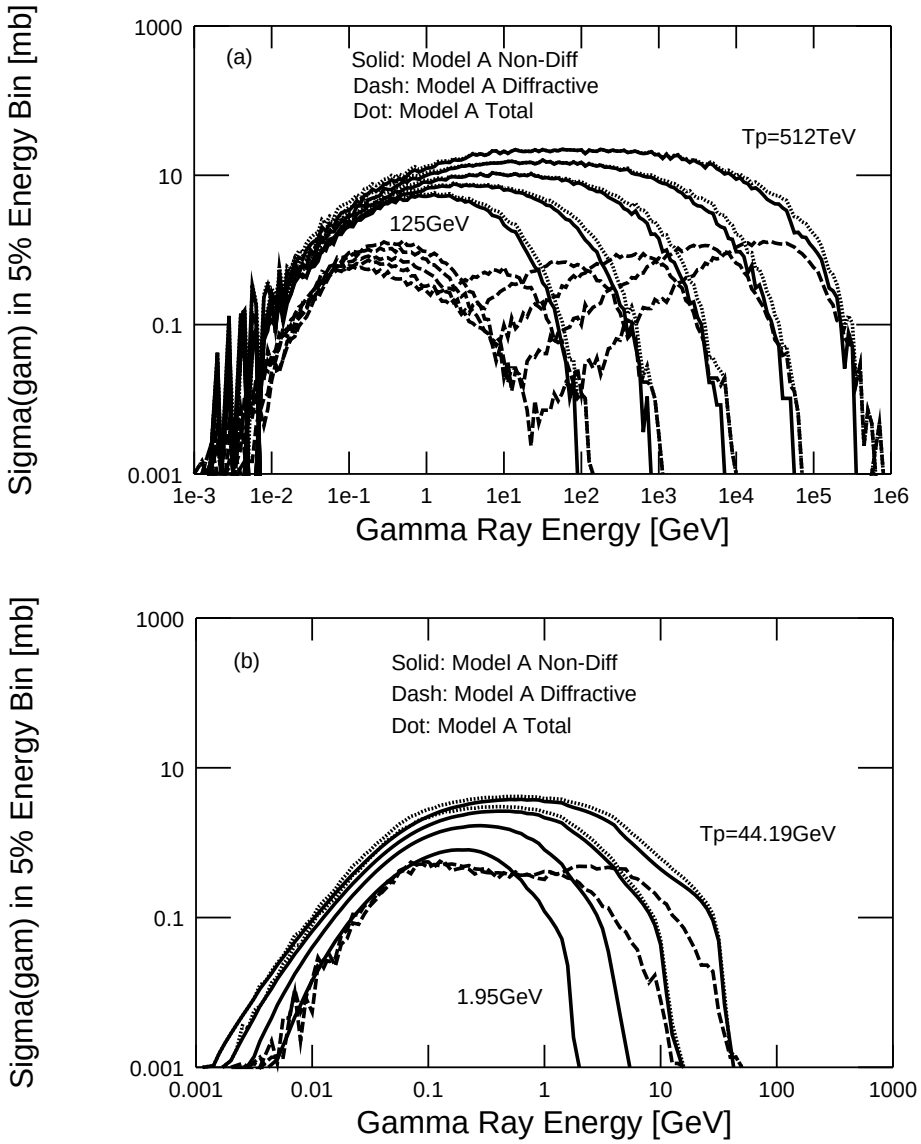

Fig. 11.— Inclusive gamma-ray cross-section per $\Delta E_\gamma = 0.05 E_\gamma$ bin for mono-energetic proton beams: model A non-diffractive (*solid curve*), model A diffractive (*dashed curve*), and model A total (*thin dotted curve*). Proton kinetic energies (T_p) are, from right to left: (a) 512 TeV, 64 TeV, 8 TeV, 1 TeV, and 125 GeV; (b) 44.19 GeV, 15.63 GeV, 5.52 GeV, and 1.95 GeV. Note that the diffractive contributions give double humps at higher energies. Also note that the cross-section for the diffractive process is zero for $T_p = 5.52$ GeV and 1.95 GeV.

REFERENCES

Affolder, T., et al. 2001, Phys. Rev. Lett., 87, 141802

Akimov, Y., et al. 1975a, Phys. Rev. Lett., 35, 763

Akimov, Y., et al. 1975b, Phys. Rev. Lett., 35, 766

Akimov, Y., et al. 1976, Phys. Rev., D14, 3148

Alberi, G., and Goggi, G. 1981, Phys. Reports, 74, 1

Albrow, M.G., et al. 1974a, Phys. Lett., B51, 421

Albrow, M.G., et al. 1974b, Phys. Lett., B51, 424

Albrow, M.G., et al. 1976, Nucl. Phys., B108, 1

Alpgard, K., et al. 1983, Phys. Lett., B121, 209

Alner, G. J., et al. 1984, Phys. Lett., B138, 304

Altarelli, G., and Parisi, G. 1977, Nucl. Physics, B126, 298

Amaldi, U., et al. 1978, Nucl. Phys., B145, 367

Andersson, B., Gustafson, G., and Peterson, C. 1979, Z. Physik, C1, 105

Andersson, B., Gustafson, G., and Sjöstrand, T. 1980, Z. Physik, C6, 235

Andersson, B. 1998, "The Lund Model", Cambridge Univ. Press

Ansorge, R. E., et al. 1989, Z. Physik, C43, 357

Asaoka, Y., et al. 2002, Phys. Rev. Lett., 88, 051101

Basini, G., et al. 1999, Proc. 26th Int. Cosmic Ray Conf. (Salt Lake City), 3, 77

Baksay, L., et al. 1978, Nucl. Phys., B141, 1

Bertsch D.L. et al. 1993, ApJ, 416, 587

Bignami, G.F., et al. 1975, Space Science Instrum. 1, 245

Bjorken, J.D. 1969, Phys. Rev., 179, 1547

Blattnig, S. R., et al. 2000, Phys. Rev., D62, 094030

Bloemen, J.B.G.M., et al. 1984, A&A, 135, 12

Bloemen, J.B.G.M. 1985, A&A, 145, 391

Boezio, M., et al. 2001, ApJ, 561, 787

Breakstone, A., et al. 1984 Phys. Rev., D30, 528

Büsching, I., Pohl, M., and Schlickeiser, R. 2001 A&A, 377, 1056

Cesarini, A., et al. 2004, Astroparticle Phys., 21, 267

Collins, P.D.B., and Martin, A.D. 1984, "Hadron Interactions", Adams Hilger

Cool, R.L., et al. 1982, Phys. Rev. Lett., 48, 1451

Corcella, G., et al. 2002, "Herwig 6.5 Release Note", hep-ph/0210213

Coutu, S., et al. 1999, Astroparticle Phys., 11, 429

Dao, F. T., Gordon, D. and Lach, J., Phys. Lett. 45, 513

de Boer, W., et al. 2003, hep-ph/0312037

Dermer, C. D. 1986, A&A, 157, 223

Donnachie, A., and Landshoff, P.V. 2004, hep-ph/0402081

Eggert, K., et al. 1975, Nucl. Physics, B98, 73

Ellison, D. C., Decourchelle, A., and Ballet, J., 2004, A&A, 413, 189

Feinberg, E.L., and Pomerancuk, Ia.I. 1956, Suppl. Nuovo Cimento III, 652

Feynman, R.P. 1969, in "High Energy Collisions" (eds.) Yang, C.N. et al., (Gordon and Breach) 237

Feynman, R.P. 1972, "Photon Hadron Interactions", Benjamin

Field, R.D. 2002, Matrix Element and Monte Carlo Tuning Workshop, $http://cepa.fnal.gov/CPD/MCTuning$, $http://www.phys.ufl.edu/\ rfield/cdf$

Ginzburg, V.L. 1967, "The Astrophysics of Cosmic Rays" Nuaka (in Russian) and NASA-TT-F561 (English translation)

Givernaud, A., et al. Nucl. Phys., B152, 189.

Good, M.L., and Walker, W.D. 1960, Phys. Rev., 120, 1855

Goulinanos, K. 1983, Phys. Reports, 101, 169

Goulinanos, K. 1995, Phys. Lett., B358, 379

Goulinanos, K., and Montanha, J. 1999, Phys. Rev., D59, 114017

Guillaud, J. P., and Sobol, A., 2004, Internal Report of Laboratoire d'Annecy-le-Vieux de Physique des Particules, LAPP-EXP 2004-06 posted at http://wwwlapp.in2p3.fr/

Hagiwara, K., et al. 2002, Phys. Rev., D66, 010001.

Hartman, R.C., et al. 1999, ApJ, 123, 79

Hayakawa, S. 1969, Sec. 6.8.2 and 6.8.3 of "Cosmic Ray Physics" John-Wiley

Hunter, S.D., et al. 1997, ApJ, 481, 205

Koba, Z., Nielsen, H.B., and Olesen, P. 1972, Nucl. Phys., B40, 317

Konishi, K., Ukawa, A., and Veneziano, G. 1978, Phys. Lett., B78, 243

Konishi, K., Ukawa, A., and Veneziano, G. 1979, Nucl. Physics, B157, 45

Marchesini, G., and Webber, B. 1984, Nucl. Phys., B238, 1

Mayer-Hasselwander, H.A., et al. 1982, A&A, 105, 164

Mori, M. 1997, ApJ, 478, 225

Moskalenko, I.V., Strong, A.W., Ormes, J.F., and Potgieter, M.S. 2002, ApJ, 565, 280

Mrenna, S., and Richardson, P. 2003, hep-ph/0312274

Murthy, P.V.R., and Wolfendale A.W. 1993 "Gamma-ray Astronomy", Cambridge Univ. Press

Naito, T., and Takahara, F. 1994, J. Phys. G: Nucl. Part. Phys., 20, 477

Orito, S., et al. 2000, Phys. Rev. Lett., 84, 1078

Perl, M.L. 1974, "High Energy Hadron Physics", John Wiley & Sons

Pohl, M., et al. 1997, ApJ, 491, 159

Schlickeiser, R. 2002, "Cosmic Ray Astrophysics", Springer Verlag

Schoenfelder, V. 2001, "The Universe in Gamma Rays", Springer Verlag

Sjöstrand, T., and van Zijl, M. 1987 Phys. Rev., D36, 2019

Sjöstrand, T., and Seymour, M.H. 1999, in Fernandez, E. & Pacheo, A. (eds.), Proc. Worldwide Study on Physics and Experiments with Future e^+e^- Colliders (Univ. Autonoma de Barcelona, 2000). Also available as hep-ph/9909346.

Sjöstrand, T., Lonnblad, L., and Mrenna, S. 2001, "Pythia 6.2: Physics and Manual", hep-ph/0108264

Sjöstrand, T., and Skands, P. Z. 2004, hep-ph/0402078

Stecker, F. 1989, in Shapiro, M.M., and Wefel, J.P. (eds.), "Cosmic Gamma Rays, Neutrinos and Related Astrophysics", p.89

Stephens, S.A., and Badhwar, G.D. 1981, Astrophys. Space Sci, 76, 213

Strong, A.W., et al. 1978, MNRAS, 182, 751

Strong, A.W., et al. 1982, A&A, 115, 404

Strong, A.W., and Moskalenko, I.V. 1997, Proc. Fourth Compton Symp., (eds) Dermer, C. D., Strickman, M. S., and Kurfess, J. D., p.1162; astro-ph/9709211

Strong, A. W., Moskalenko, I. V., and Reimer, O. 2000, ApJ, 537, 763; Errortum: 2000, ibid, 541, 1109

Strong, A. W., and Moskalenko, I. V. 2001, Proc. of 27th ICRC 2001 (Hamburg), p.1942 and astro-ph/0106504

Strong, A. W., Moskalenko, I. V., and Reimer, O. 2004, ApJ, 613 (in press) and astro-ph/0406254

Thompson, D.J., et al. 1993, ApJS, 86, 629

Webber, B.R. 1984, Acta Phys. Polon., B15, 617

Webber, B.R. 1984, Nucl. Phys., B238, 492

This preprint was prepared with the AAS LaTeX macros v5.2.